Applied Catalysis B: Environmental 207 (2017) 397–403

Contents lists available at ScienceDirect

Applied Catalysis B: Environmental

journal homepage: www.elsevier.com/locate/apcatb

# Remarkable synergistic effect between {001} facets and surface F ions promoting hole migration on anatase $TiO_2$

Min Chen[a,b], Jinzhu Ma[a,b,c], Bo Zhang[a,b], Guangzhi He[a,b], Yaobin Li[a,b,c], Changbin Zhang[a,b,*], Hong He[a,b,c]

[a] State Key Joint Laboratory of Environment Simulation and Pollution Control, Research Center for Eco-Environmental Sciences, Chinese Academy of Sciences, Beijing 100085, China
[b] University of Chinese Academy of Sciences, Beijing 100049, China
[c] Center for Excellence in Regional Atmospheric Environment, Institute of Urban Environment, Chinese Academy of Sciences, Xiamen 361021, China

ARTICLE INFO

*Article history:*
Received 28 October 2016
Received in revised form 7 February 2017
Accepted 12 February 2017
Available online 14 February 2017

*Keywords:*
Photocatalysis
Exposed facet
$TiO_2$
Surface fluorine
$NH_3$ oxidation

ABSTRACT

Controllable synthesis and surface modification of $TiO_2$ crystals with specific exposed facets using fluoride as a shape directing agent have drawn a great deal of attention in the photocatalytic field. Both the exposed facets and surface F ions are known to have a great influence on the photocatalytic performance of $TiO_2$ crystals, while these two factors are usually considered and discussed separately. Here, we investigated the influence of surface F ions on the carrier migration when the surface F ions are present on anatase $TiO_2$ crystals with predominant {001} or {101} facets by using the $H_2O$ photo-oxidation and $NH_3$ photo-oxidation as the probe reactions. We observed a remarkable synergistic effect between {001} facets and surface F ions on the photogenerated hole migration. The {001} facets provide hole-trapping sites and the electrostatic effect of surface F anions attract and accelerate the holes migration to {001} facets, which synergistically promote the electron-hole pair separation and thus significantly enhance the photo-oxidation activity. However, no synergistic effect was detected between {101} facets and the surface F ions. This finding provides a new insight into the photogenerated charge migration on fluorinated $TiO_2$ with specific exposed facets.



## 1. Introduction

Nanocrystalline $TiO_2$ is a chemically stable nontoxic photocatalytic material that has been widely studied because of its potential application in water and air purification, $H_2$ evolution from water, etc [1–4]. In particular, anatase phase $TiO_2$ has been undoubtedly proved to be the most photoactive among the various $TiO_2$ crystallographic phases [1,2,5,6]. The reactivity of anatase $TiO_2$ photocatalyst with a wide band gap (3.2 eV) is attributed to photogenerated electrons ($e^-$) and holes ($h^+$), located at the crystal surface, where they initiate various redox reactions of the adsorbed substances [2,6]. During the transportation processes of photogenerated carriers, a substantial portion of carriers are lost due to electron-hole recombination. Trapping of photogenerated holes by $H_2O$ or trapping of photogenerated electrons by $O_2$ is apparently a crucial step in the process of charges separation [1,2,6,7]. Among the various factors affecting the migration of charges, the surface properties of $TiO_2$ such as crystal facets [8–10], surface defects [11–13], and surface adsorbed anion or cation [14,15] exert a dominant influence.

Modification and morphological control of $TiO_2$ crystal facets has drawn much attention since the synthesis of anatase $TiO_2$ with high percentage of exposed {001} facets was first achieved [9], and intensive efforts have been made to controllably synthesize anatase $TiO_2$ with specific exposed facets [16–21]. Recently, an increasing number of reports suggest that the photocatalytic activity is closely related to the specific exposed facets [22–29]. For instance, Han et al. [26] found that {001} facets show higher photodegradative activity for organic pollutants than {101} facets, while Pan et al. [27]. pointed out that {101} and {010} facets exhibit photo-activity superior to {001} facets for the $H_2$ evolution reaction. Conventionally, anatase $TiO_2$ favors the exposure of {101} facets because of its low surface energy (0.44 $J/m^2$). The {001} facets (0.9 $J/m^2$) is considered to be 100% 5-fold coordinated titanium atoms ($Ti_{5c}$) compared with 50% $Ti_{5c}$ on the {101} surface, which tends to be high photocatalytic activity [9]. It is also be pointed out that the specific exposed

* Corresponding author at: State Key Joint Laboratory of Environment Simulation and Pollution Control, Research Center for Eco-Environmental Sciences, Chinese Academy of Sciences, Beijing 100085, China.
*E-mail address:* cbzhang@rcees.ac.cn (C. Zhang).

http://dx.doi.org/10.1016/j.apcatb.2017.02.048
0926-3373/

facets of $TiO_2$ nanocrystals greatly affect the trapping and interfacial transfer of photogenerated charges. {001} facets of anatase $TiO_2$ favor the trapping of holes as oxidative sites, while {101} facets incline to trap electrons as reductive sites [30,31].

By using fluoride as a shape directing agent during the synthesis of anatase $TiO_2$ with different exposed facets, surface F ions are inevitably introduced into anatase $TiO_2$. It has been documented that introduced surface F ions also modify photocatalytic activity by acting as electron-trapping sites [32,33], by promoting the adsorption of oxygen [34], or by accelerating the holes movement to $TiO_2$ surface [35]. Very recently, Chen et al. [36] found that surface $H_2O$ are greatly oxidized by photogenerated holes when terminal F and lattice F replacing surface bridging oxygen coexist on {101} facets of anatase $TiO_2$. However, in previous reports, the effects of specific exposed facets and surface F ions on charges migration were usually investigated and discussed separately. It remains to be demonstrated whether the influence of F ions on the carrier migration and also on photocatalytic activity is dependent on the exposed facets of $TiO_2$ crystals.

Here, by means of in situ diffuse reflectance infrared Fourier transform spectroscopy (DRIFTS) using $H_2O$ oxidation and $NH_3$ oxidation as the probe reactions, we investigated the properties of photogenerated holes transfer over fluorinated $TiO_2$ with specific exposed facets ({001} or {101}) at room temperature. A dramatic synergistic effect between the exposed {001} facets and surface F ions was observed, which greatly promotes the hole migration, therefore significantly enhancing the photo-activity for the hole-sensitive reaction, such as $H_2O$ oxidation and $NH_3$ oxidation, while no synergistic effect existed between the exposed {101} facets and surface F ions.

## 2. Experimental

### 2.1. Sample synthesis

The fluorinated $TiO_2$ with exposed {001} facets (denoted as F-T001) was controllably prepared according to a modified HF hydrothermal method similar to that reported by Han et al. [26] In a typical synthesis, 4 mL of hydrofluoric acid solution (40 wt.%) was added dropwise into the prepared $Ti(OC_4H_9)_4$ (25 mL) in a 100 mL Teflon-lined autoclave at room temperature under magnetic stirring, then the autoclave was sealed and heated at 190 °C for 24 h. After hydrothermal reaction, the white precipitate was collected and washed with ethanol and distilled water several times, and finally dried overnight in an oven at 60 °C. In order to defluorinate the F-T001 sample (labeled as T001), 1 g of the obtained F-T001 powder was subsequently washed with 0.1 M NaOH solution.

The octahedral {101} facets-exposed $TiO_2$ particles (T101) were synthesized by a two-step hydrothermal procedure similar to previous reports [37,38]. In the first step, 1 g of P25 was reacted hydrothermally with 70 mL KOH solution (10 M) in a Teflon-lined autoclave with a capacity of 100 mL at 200 °C for 48 h. The resulting precipitate was washed and neutralized using deionized water and dried at 60 °C. In the second step, the prepared potassium titanate (70 mg) was stirred in distilled water (70 mL) and heated in a 100 mL Teflon-lined autoclave at 170 °C for 24 h. The white precipitate was washed and dried at 100 °C.

The fluorination of T101 (T101-F) was obtained by HF solution treatment according to a previous report [28]. 0.5 g of T101 was dispersed in HF aqueous solution (5 wt%), and the solution was stirred for 0.5 h at room temperature. The resulting powder was washed with deionized water several times and dried at 60 °C for 6 h. T001 was also treated by the same method to obtain T001-F.

### 2.2. Material characterization

Powder X-ray diffraction (XRD) measurements of the catalysts were carried out on an X'Pert PRO MPD X-ray powder diffractometer (Japan) using Cu Kα radiation operating at 40 kV and 40 mA. The patterns were measured over the 2θ range from 10° to 90° with a scan step size of 0.02°. The specific surface area of the catalysts was obtained at 77 K over the whole range of relative pressures, using a Quantachrome Quadrasorb SI-MP analyzer. Field emission scanning electronic microscopy (FE-SEM) measurements were performed on a SU-8020 electron microscope (Hitachi, Japan). Transmission electron microscopy (TEM) and high-resolution transmission electron microscopy (HRTEM) images were obtained on a JEM-2011 electron microscope (JEOL, Japan). The surface composition and VB-XPS spectra of the samples were examined by X-ray Photoelectron Spectroscopy (XPS) using a scanning X-ray microprobe (AxisUltra, Kratos Analytical Ltd.) using Al K-α radiation (1486.7 eV). The C1 s peak (284.8 eV) was used to calibrate the binding energy (BE) values.

In situ diffuse reflectance infrared Fourier transform spectroscopy (DRIFTS) was used to study the photochemical properties of photocatalysts. A Fourier transform infrared spectrometer (Nicolet 380) equipped with a MCT detector was used to collect the infrared spectra in the range of 4000–800 $cm^{-1}$ by averaging 32 scans with a resolution of 4 $cm^{-1}$ at scanning velocity of 20 kHz. The reaction cell housing a sample cup was filled with the photocatalysts. The cover dome has three windows, where two are ZnSe windows used for entry and exit of the detection infrared beam. The third quartz window is for the transmission of UV light during in situ photoreactions. In $H_2O$ oxidation experiments, $N_2$ flows (RH 50%, 100 mL/min) were firstly introduced to reach the adsorption saturation of water on catalyst surface, then the flows were switched to pure $N_2$ for 60 min as the background, finally UV irradiation was introduced and IR changes were recorded.

### 2.3. $NH_3$ oxidation activity test

The photocatalytic experiments for the removal of $NH_3$ were performed at ambient temperature in a home-made flow reactor. The cylindrical reactor was made of stainless steel and covered with a quartz plate. A sample dish containing the photocatalyst powders was placed in the center of the reactor, and 0.07 g of photocatalyst was used for each evaluation experiment. A 500 W commercial Hg lamp (Beijing TrusTech Science and Technology Co., China) was used as the light source with an optical filter (λ=365–366 nm), and the average light intensity was 12 mW/$cm^2$. The lamp was vertically placed outside the reactor above the sample dishes, and the temperature of the sample was kept at 25 °C by water circulation. The relative concentrations of effluent gas, including $NH_3$, NO, $NO_2$ and $N_2O$, were continuously measured by an FTIR spectrometer (Nicolet 380) equipped with 2 m gas cell and a DTGS detector. The surface $NO_3^-$ deriving from $NH_3$ oxidation was quantified by ion chromatography (ICS-2100). The reactant gas circularly flowed over the catalyst, and the initial reactant gas was 500 ppm $NH_3$, 20 vol% $O_2$, RH 50%, and $N_2$ balance.

## 3. Results and discussion

The crystallographic structures of the as-synthesized samples were confirmed by XRD measurements. As shown in Fig. 1, all samples exhibited the standard anatase XRD patterns [JCPDS no. 21-1272, space group: I41/amd (141)]. F-T001 showed a broad {004} peak as well as a narrow {200} peak, indicating that the crystal growth is limited mainly to the {001} axis [39,40]. The stronger intensities and narrower widths of the XRD peaks in T101 revealed

**Table 1**
Physiochemical Properties of F-T001, T001, T001-F, T101-F and T101.

| Sample | Morphology | SSA($m^2$/g) | Crystal size [a](nm) | Predominant facet [b] (%) | Bandgap [c] (eV) | F content [d] (atom%) |
|---|---|---|---|---|---|---|
| F-T001 | nanosheets | 86 | 15.1 | 68.9 | 3.23 | 4.2 |
| T001 | nanosheets | 84 | 15.9 | 68.7 | 3.23 | – |
| T001-F | nanosheets | 82 | 15.3 | 68.2 | 3.23 | 3.2 |
| T101-F | nanoctahedra | 41 | 48.8 | 90.2 | 3.27 | 2.7 |
| T101 | nanoctahedra | 43 | 50.4 | 90.3 | 3.27 | – |

[a] Crystal size was calculated by the half-width of {101} peaks using the Scherer formula.
[b] Predominant facet percentage was estimated by SEM images.
[c] Bandgap of samples were measured by UV-vis spectra.
[d] F content of samples were determined by XPS.

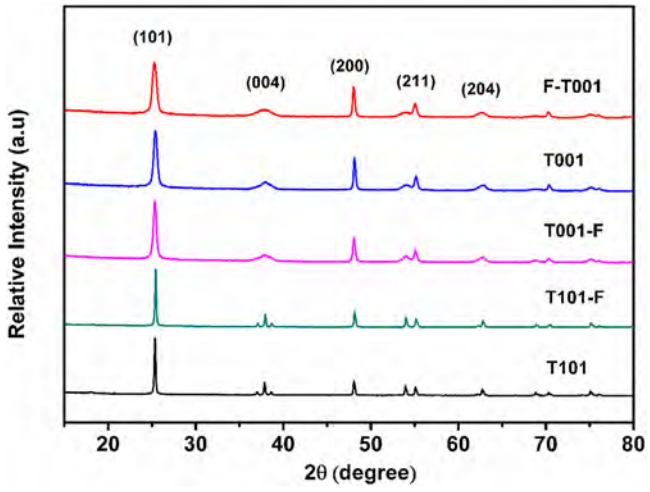


**Fig. 1.** The powder X-ray diffraction patterns of synthesized samples at room temperature.

the good crystallinity. In addition, it is noteworthy that the process of defluorination or fluorination has no impact on the XRD patterns of F-T001 or T101. The crystal sizes of samples were calculated from the half-width of {101} peaks using the Scherrer formula and the results are given in Table 1.

Representative SEM images of the samples are shown in Fig. 2. F-T001 and T001 were composed of nearly identical nanosheets, while T101-F and T101 displayed nearly uniform nanooctahedral. It is clearly that the defluorination or fluorination process does not have a significant impact on the morphologies of T101-F and T101. In order to identify the exposed facets of the prepared samples, high resolution transmission electron microscopy (HR-TEM) images were obtained and analyzed (Fig. 3). In the case of the F-T001, the lattice spacing parallel to the top and bottom facets was ca. 0.235 nm, corresponding to the {001} planes of anatase $TiO_2$, which is consistent with previous reports [19,39,40]. T101-F showed another set of the lattice fringes with spacing of 0.35 nm, corresponding to the {101} planes of anatase $TiO_2$ [23]. The average percentages of the {001} or {101} facets were calculated based on the morphology of the samples. The percentages of {001} exposed crystal facets for F-T001, T001 and T001-F were estimated at 69%, and the percentages of {101} for T101 and T101-F were at around 90%. Considering the variations in particle size and dimensions, the specific surface area (SSA) of the samples was also measured. As shown in Table 1, the BET surface areas of nanosheet samples were calculated to be about 84 $m^2\ g^{-1}$, roughly two times as high as those of the nanoctahedra samples. Furthermore, the bandgaps of the samples were measured by UV–vis diffuse reflectance spectroscopy (Fig. S1). The F-T001, T001 and T001-F exhibited identical bandgaps with a value of approximately 3.23 eV, and T101 and T101-F both showed the bandgaps of 3.27 eV, which are similar with previous

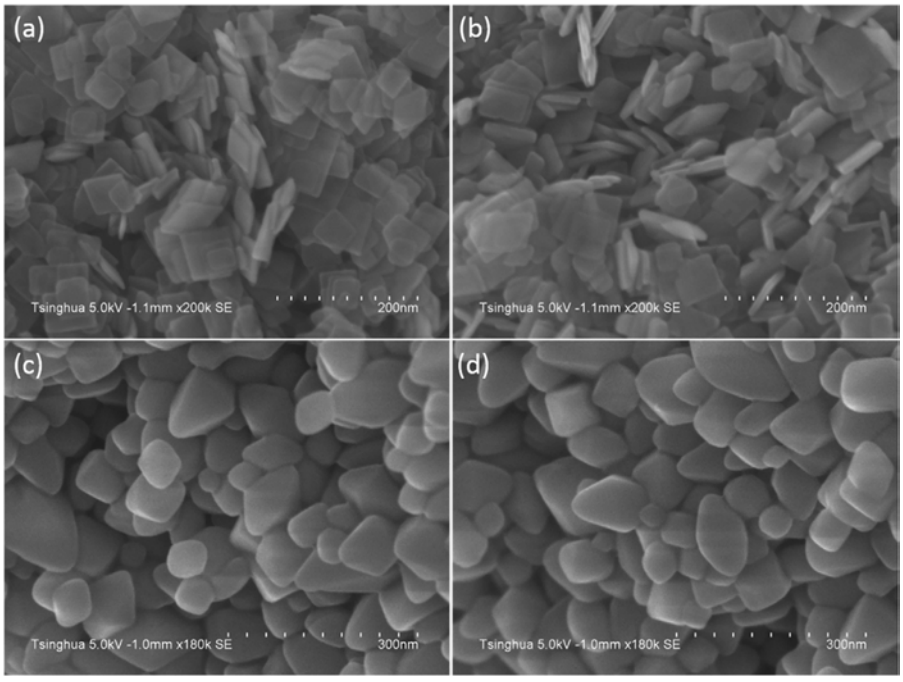


**Fig. 2.** SEM images of as-synthesized samples. (a) F-T001; (b) T001; (c) T101-F; (d) T101.

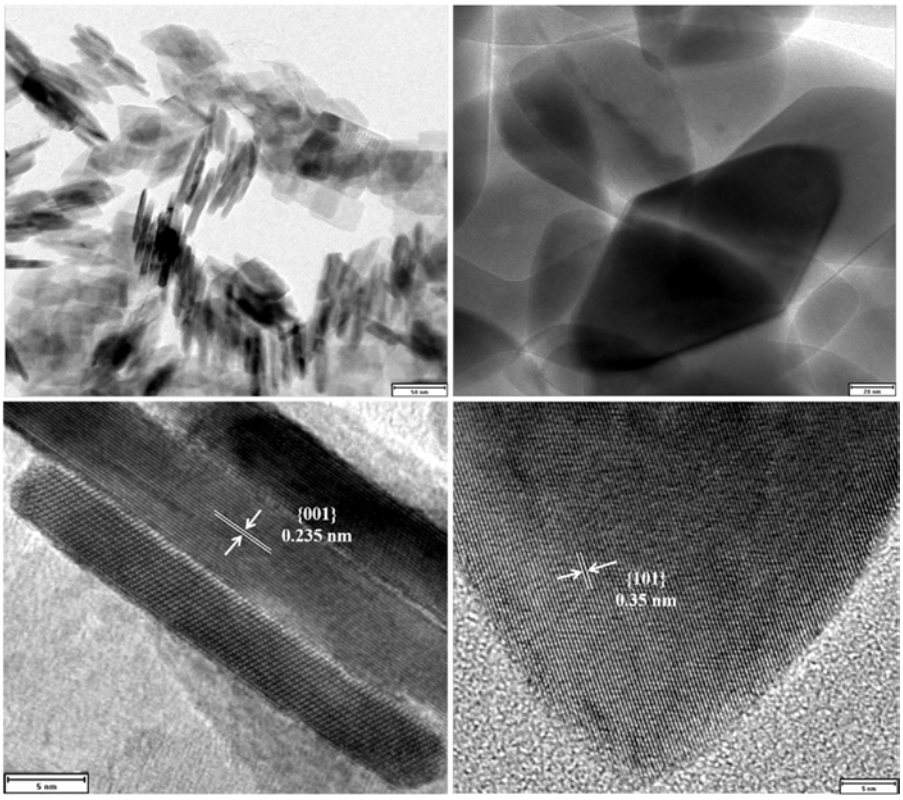


**Fig. 3.** TEM (top) and HRTEM (bottom) images of F-T001 (left) and T101-F (right).

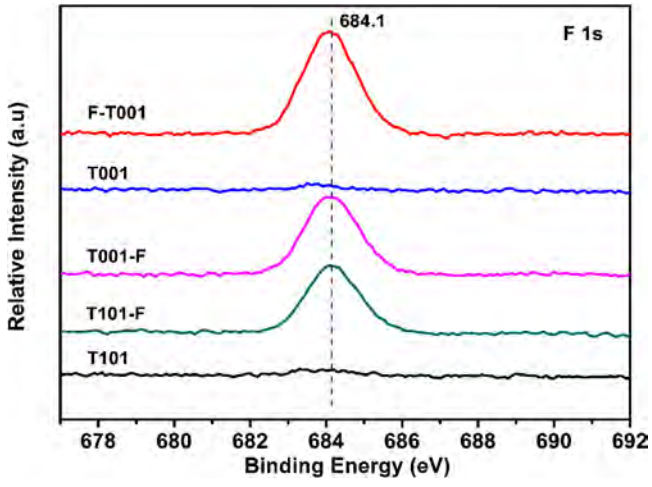


**Fig. 4.** High resolution F 1 s XPS spectra of the samples.

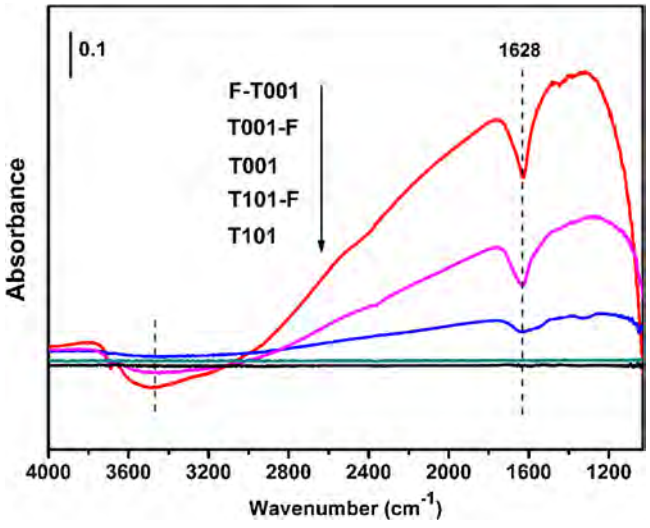


**Fig. 5.** IR spectra of F-T001, T001, T001-F, T101-F and T101 after 5 min UV irradiation under $N_2$ atmosphere.

reports [25,38]. The VB position of the nanosheets and nanooctahedral samples are at about 1.9 eV below the Fermi energy and are nearly identical to each other (Fig. S2). The detailed information of physiochemical properties of the samples are summarized in Table 1.

XPS spectra were next performed to obtain the chemical binding energy of F atoms. As shown in Fig. 4, F 1 s peaks at 684.1 eV were observed in F-T001, T001-F and T101-F samples, indicating that F ions acting as a shape directing agent are strongly bound to the {001} or {101} surface by forming ≡Ti—F bonds [32,40]. No signal of fluorine substituting for surface bridging oxygen (BE 688.5 eV) was detected [36]. The F contents of the samples were calculated and presented in Table 1. The results show that the F contents in F-T001, T001-F and T101-F was 4.2%, 3.2% and 2.7%, respectively.

DRIFTS has proven to be a powerful tool to monitor the transfer of the photogenerated carriers in semiconductor photocatalysis [36,41–43]. In the present work, $H_2O$ oxidation was first chosen as a probe reaction to investigate the migration of photogenerated holes. On one hand, photogenerated holes can react with surface adsorbed $H_2O$ while photogenerated electrons cannot. On the other hand, the accumulation of electrons on the $TiO_2$ surface resulting from $H_2O$ oxidation by holes can usually absorb mid-IR (MIR) light and thus can be monitored using IR spectroscopy. As shown in Fig. 5, in the presence of $H_2O$, the UV irradiation caused no change in the IR spectra of T101 and T101-F, and no additional adsorption peaks appeared. Intriguingly, in the case of

the F-T001, the UV irradiation induced a remarkable increase in a structureless background IR absorbance band ranging from 3000 to 1000 $cm^{-1}$, which is attributed to electron accumulation in the conduction band. In addition, a broad negative absorption band ranging from 3700 to 3000 $cm^{-1}$ and narrow negative peak at 1628 $cm^{-1}$ appeared, which are assigned to $\nu$ (OH) and $\delta$ ($H_2O$), respectively [36], indicating that the surface adsorbed $H_2O$ on F-T001 is oxidized and consumed by photogenerated holes under UV irradiation. In contrast, the electrons accumulation and surface adsorbed $H_2O$ consumption significantly decreased for T001 due to the removal of surface F ions. When surface F ions were re-introduced on T001, $H_2O$ oxidation clearly recovered on the T001-F sample to a large degree. Our DRIFTS results revealed that no $H_2O$ oxidation occurred on the T101 and T101-F samples under UV irradiation, in which the electron-hole pairs rapidly recombined. However, when the {001} facets cooperated with surface F ions, more photogenerated holes were driven to the surface to oxidize the $H_2O$, resulting in significant electron accumulation, demonstrating that the separation of electron-hole pairs was dramatically promoted.

In order to further confirm the synergistic effect between {001} facets and surface F ions, we compared the photocatalytic oxidation activities of the samples in the photocatalytic oxidation of gaseous $NH_3$. Generally, active species including $h^+$, $^\bullet OH$, $^\bullet O_2^-$ are all involved in photocatalytic oxidation reactions and they often work together [6,44–46]. Among them, $^\bullet O_2^-$ originates from the transfer of photogenerated electrons to surface $O_2$, and $^\bullet OH$ derives both from $H_2O$ oxidation by $h^+$ and transformation of $^\bullet O_2^-$ [6]. Thus, it is hard to accurately evaluate the migration of photogenerated $h^+$ by direct measurement of $^\bullet OH$, and $^\bullet O_2^-$ species. Our DFT calculations results (Fig. S2) show that $NH_3$ cannot be oxidized by $^\bullet O_2^-$. Previous studies and the NIST database show that the oxidation of $NH_3$ by $^\bullet OH$ is extremely slow due to the low reaction rate constant [47]. In contrast, the reaction of $NH_3$ with a valence band hole on the $TiO_2$ surface has been demonstrated by ESR [48]. According to previous reports, the rate of surface $NH_3$ photo-oxidation is much slower than the rate of $NH_3$ adsorption on $TiO_2$ [48–53], indicating that the $NH_3$ photo-oxidation process is the rate-determining step for this reaction. In addition, $TiO_2$ as an acidic oxide can well adsorb $NH_3$, thus the capacities of $NH_3$ adsorption on above $TiO_2$ samples do not have a strong influence on their activity for $NH_3$ photo-oxidation. Therefore, the $NH_3$ photo-oxidation is a hole-sensitive reaction, and it can be feasibly applied to evaluate the migration of photogenerated holes on different samples.

The photocatalytic oxidation of $NH_3$ over the samples was performed in the presence of UV irradiation. Before UV irradiation, $NH_3$ was flowed over catalyst in the dark for 2 h to reach $NH_3$ adsorption-desorption equilibrium on catalyst surface. The test results are presented in Fig. 6a. The $NH_3$ conversion was negligible under UV irradiation in the absence of a photocatalyst. The concentration ratio log ($C/C_0$) of $NH_3$ plotted against UV irradiation time in the presence of catalysts showed a pseudo-first-order kinetics to the $NH_3$ concentration, where "$C_0$" and "C" are the $NH_3$ concentration before and after irradiation, respectively. Given the differences in specific surface areas (SSA) among the samples, we calculated the specific $NH_3$ conversion rate constants ($m^2_{catalyst}$ min)$^{-1}$ according to the first-order dynamic equation ($\frac{dC_{NH_3}}{dt} = kC_{NH_3}$) and the results are shown in Fig. 6b. As shown in Fig. 6b, the in-situ synthesized F-T001 exhibited the highest $NH_3$ oxidation activity ($9.5 \times 10^{-4}$) among the samples. When the surface F ions of F-T001 were removed (T001), the $NH_3$ oxidation activity greatly decreased. After surface F ions were re-introduced on T001, the activity largely recovered (T001-F). F-T001 exhibited slightly higher $NH_3$ oxidation activity than T001-F, so this may be due to more surface F ions were present on F-T001 (Fig. 4). In contrast, T101 presented a very low $NH_3$ conversion rate ($1.1 \times 10^{-4}$), and the T101-F showed a nearly

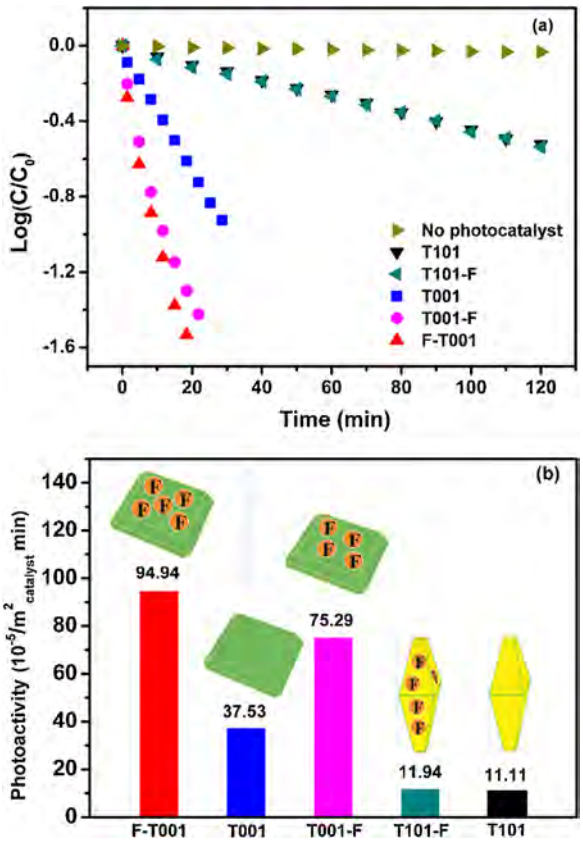


**Fig. 6.** Photocatalytic oxidation of $NH_3$ (a) log ($C/C_0$) vs reaction time (b) rate constants compare under UV irradiation over F-T001, T001, T001-F, T101-F and T101.

identical activity as compared to T101. These results further proved the presence of a synergistic effect between {001} facets and surface F ions on hole migration. Product analysis was also carried out for the F-T001 sample. It is shown that only a small amount of $N_2O$ (7 ppm) was detected in gas phase products (Fig. S4). We further measured the $NO_3^-$ species adsorbed on the F-T001 surface by ion chromatography, and found that about 13 percent of $NH_3$ are converted into $NO_3^-$ species (Table S1). Therefore, the $N_2$ selectivity the F-T001 sample was calculated to be about 84%, which is in agreement with the reported results [48–50].

The question then arises as to why the fluorinated $TiO_2$ with exposed {001} or {101} facets displayed such a dramatic difference in photogenerated charge transfer. Apparently, two key factors involving surface F ions and facet effect should be taken into account. In a very recent report, Chen et al. [36] systematically discussed the roles of surface F ions over {101} facets on the photocatalytic process. They found that only when terminal F and lattice F co-exist on {101} facets, the surface $H_2O$ can be oxidized by photogenerated holes under UV irradiation, while terminal F or lattice F exist alone caused no surface $H_2O$ oxidation. In fact, our XPS results demonstrated that only the surface F ions in the form of ≡Ti—F bonds were formed on the F-T001, T001-F, or T101-F samples. Our T101 and T101-F samples both showed no activity for $H_2O$ oxidation, which are in agreement with the results reported by Chen et al. [36]. Surprisingly, T001 showed a considerable activity for surface $H_2O$ oxidation compared to T101 sample, and the activity was further greatly enhanced when the terminal F ion was present on {001} facet. It is clearly suggested that the influence of F ions on the carrier migration is closely dependent on the exposed facets of $TiO_2$ crystals.

It has been reported that photogenerated holes are inclined to migrate to {001} facets as oxidative sites, while photogener-

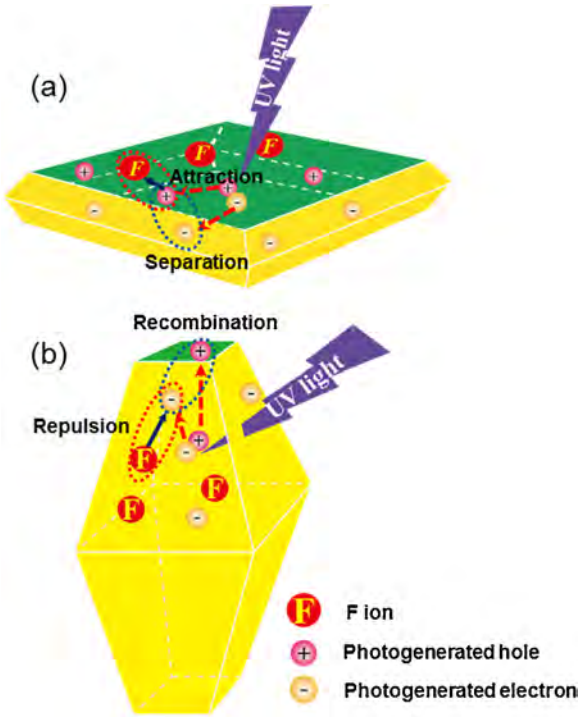


**Fig. 7.** Schematic illustration of the likelihood of charges migration on fluorinated {001} facets (a) and {101} facet (b).

ated electrons tend to migrate to {101} facets as reductive sites [30], thereby rendering {001} facets more active for photooxidation reactions than {101} facets. Surface F ions, as anions on the $TiO_2$ surface, form a negative electric field, drawing the photogenerated holes to move to the surface by the electrostatic force [35]. As illustrated in Fig. 7. When surface F ions are present on {001} facets, the facets provide more hole-trapping sites, and the surface F ions drive the movement of the positively charged holes to the {001} surface, resulting in a synergistic promotion effect between {001} facets and surface F ions on electron-hole pairs separation. In contrast, when the surface F ions are present on {101} facets, the effects of {101} facets and the surface F ions on charges migration are opposite. Photogenerated electrons tend to migrate on {101} facets; however, the surface F anion electrostatic effect could suppress the migration of photogenerated electrons, which favored electron-hole recombination. Related research also found that surface F anion modification reduced the $H_2$ evolution photoactivity over $TiO_2$ crystals [27], which may be due to the decreased migration of photogenerated electrons by F ions presence. In this work, we did not detailedly discuss the role of photogenerated electrons since the photogenerated electrons is not a key factor in $H_2O$ and $NH_3$ oxidation. Our recent study have found that $^{\bullet}O_2^-$ radical formed by trapping photogenerated electrons may paticipate in the subsequent oxidation of $NH_3$ (not first step), and the results will be reported in our next work.

## 4. Conclusions

Based on the results of DRIFTS experiments for $H_2O$ oxidation and the testing for hole-sensitive $NH_3$ oxidation over fluorinated $TiO_2$ with specific exposed facets, we found a remarkable synergistic effect between {001} facets of anatase $TiO_2$ crystals and surface F ions on hole migration, while no such a synergistic effect exists between {101} facets and surface F ions. The {001} facets provide hole-trapping sites and the electrostatic effect of surface F anions attract and accelerate the holes migration to {001} facets, thus significantly enhancing the photo-oxidation activity. This finding provides a new insight into the photogenerated charge migration of fluorinated $TiO_2$ with specific exposed facets.

## Acknowledgments

This work was financially supported by the National Natural Science Foundation of China (21422706, 21577159), the Strategic Priority Research Program of the Chinese Academy of Sciences (XDB05050600) and the Youth Innovation Promotion Association, CAS (2017064). We acknowledge the useful discussion with Professor Chuncheng Chen (Key Laboratory of Photochemistry National Laboratory for Molecular Sciences, Institute of Chemistry Chinese Academy of Sciences) regarding the interpretation of DRIFTS results.

## Appendix A. Supplementary data

Supplementary data associated with this article can be found, in the online version, at http://dx.doi.org/10.1016/j.apcatb.2017.02.048.

## References

[1] A. Fujishima, X. Zhang, D. Tryk, Surf. Sci. Rep. 63 (2008) 515–582.
[2] M.R. Hoffmann, S.T. Martin, W.Y. Choi, D.W. Bahnemann, Chem. Rev. 95 (1995) 69–96.
[3] H. Yamashita, M. Harada, J. Misaka, M. Takeuchi, K. Ikeue, M. Anpo, J. Photochem. Photobiol. A 148 (2002) 257–261.
[4] H. Yamashita, Y. Ichihashi, M. Anpo, M. Hashimoto, C. Louis, M. Che, J. Phys. Chem. 100 (1996) 16041–16044.
[5] X. Chen, S.S. Mao, Chem. Rev. 107 (2007) 2891–2959.
[6] T. Tachikawa, M. Fujitsuka, T. Majima, J. Phys. Chem. C 111 (2007) 5259–5275.
[7] C. Chen, W. Ma, J. Zhao, Chem. Soc. Rev. 39 (2010) 4206–4219.
[8] G. Liu, H.G. Yang, J. Pan, Y.Q. Yang, G.Q. Lu, H.M. Cheng, Chem. Rev. 114 (2014) 9559–9612.
[9] H.G. Yang, C.H. Sun, S.Z. Qiao, J. Zou, G. Liu, S.C. Smith, H.M. Cheng, G.Q. Lu, Nature 453 (2008) 638–641.
[10] K. Lv, B. Cheng, J. Yu, G. Liu, Phys. Chem. Chem. Phys. 14 (2012) 5349–5362.
[11] M. Kong, Y. Li, X. Chen, T. Tian, P. Fang, F. Zheng, X. Zhao, J. Am. Chem. Soc. 133 (2011) 16414–16417.
[12] J. Ma, H. Wu, Y. Liu, H. He, J. Phys. Chem. C 118 (2014) 7434–7441.
[13] J. Wang, P. Zhang, X. Li, J. Zhu, H. Li, Appl. Catal. B 134-135 (2013) 198–204.
[14] D. Zhao, C.C. Chen, Y.F. Wang, H.W. Ji, W.H. Ma, L. Zang, J.C. Zhao, J. Phys. Chem. C 112 (2008) 5993–6001.
[15] W. Ren, Z. Ai, F. Jia, L. Zhang, X. Fan, Z. Zou, Appl. Catal. B 69 (2007) 138–144.
[16] T.R. Gordon, M. Cargnello, T. Paik, F. Mangolini, R.T. Weber, P. Fornasiero, C.B. Murray, J. Am. Chem. Soc. 134 (2012) 6751–6761.
[17] N. Roy, Y. Park, Y. Sohn, K.T. Leung, D. Pradhan, ACS Appl. Mater. Inter. 6 (2014) 16498–16507.
[18] N. Roy, Y. Sohn, D. Pradhan, ACS Nano 7 (2013) 2532–2540.
[19] Q. Xiang, K. Lv, J. Yu, Appl. Catal. B 96 (2010) 557–564.
[20] Y. Zhao, W. Ma, Y. Li, H. Ji, C. Chen, H. Zhu, J. Zhao, Angew. Chem. Int. Ed. 51 (2012) 3188–3192.
[21] Z. Wang, K. Lv, G. Wang, K. Deng, D. Tang, Appl. Catal. B 100 (2010) 378–385.
[22] J. Jiang, K. Zhao, X. Xiao, L. Zhang, J. Am. Chem. Soc. 134 (2012) 4473–4476.
[23] M. Wang, F. Zhang, X. Zhu, Z. Qi, B. Hong, J. Ding, J. Bao, S. Sun, C. Gao, Langmuir 31 (2015) 1730–1736.
[24] L. Ye, J. Mao, J. Liu, Z. Jiang, T. Peng, L. Zan, J. Mater. Chem. A 1 (2013) 10532–10537.
[25] L. Ye, J. Mao, T. Peng, L. Zan, Y. Zhang, Phys. Chem. Chem. Phys. 16 (2014) 15675–15680.
[26] X. Han, Q. Kuang, M. Jin, Z. Xie, L. Zheng, J. Am. Chem. Soc. 131 (2009) 3152–3253.
[27] J. Pan, G. Liu, G.Q. Lu, H.M. Cheng, Angew. Chem. Int. Ed. 50 (2011) 2133–2137.
[28] X. Yu, B. Jeon, Y.K. Kim, ACS Catal. 5 (2015) 3316–3322.
[29] J. Wang, Z. Bian, J. Zhu, H. Li, J. Mater. Chem. A 1 (2013) 1296–1302.
[30] M. D'Arienzo, J. Carbajo, A. Bahamonde, M. Crippa, S. Polizzi, R. Scotti, L. Wahba, F. Morazzoni, J. Am. Chem. Soc. 133 (2011) 17652–17661.
[31] T. Tachikawa, S. Yamashita, T. Majima, J. Am. Chem. Soc. 133 (2011) 7197–7204.
[32] M. Minella, M.G. Faga, V. Maurino, C. Minero, E. Pelizzetti, S. Coluccia, G. Martra, Langmuir 26 (2010) 2521–2527.
[33] H. Park, W. Choi, J. Phys. Chem. B 108 (2004) 4086–4093.
[34] Y. Luan, L. Jing, Y. Xie, X. Sun, Y. Feng, H. Fu, ACS Catal. 3 (2013) 1378–1385.
[35] H. Sheng, Q. Li, W. Ma, H. Ji, C. Chen, J. Zhao, Appl. Catal. B 138-139 (2013) 212–218.

[36] H. Sheng, H. Zhang, W. Song, H. Ji, W. Ma, C. Chen, J. Zhao, Angew. Chem. Int. Ed. 54 (2015) 5905–5909.
[37] F. Amano, T. Yasumoto, O.O. Prieto-Mahaney, S. Uchida, T. Shibayama, B. Ohtani, Chem. Commun. 45 (2009) 2311–2313.
[38] C. Li, C. Koenigsmann, W. Ding, B. Rudshteyn, K.R. Yang, K.P. Regan, S.J. Konezny, V.S. Batista, G.W. Brudvig, C.A. Schmuttenmaer, J.H. Kim, J. Am. Chem. Soc. 137 (2015) 1520–1529.
[39] L. Ren, Y. Li, J. Hou, J. Bai, M. Mao, M. Zeng, X. Zhao, N. Li, Appl. Catal. B 181 (2016) 625–634.
[40] H. Wu, J. Ma, Y. Li, C. Zhang, H. He, Appl. Catal. B 152-153 (2014) 82–87.
[41] S. Shen, X. Wang, T. Chen, Z. Feng, C. Li, J. Phys. Chem. C 118 (2014) 12661–12668.
[42] S.H. Szczepankiewicz, J.A. Moss, M.R. Hoffmann, J. Phys. Chem. B 106 (2002) 2922–2927.
[43] F. Guzman, S.S. Chuang, J. Am. Chem. Soc. 132 (2010) 1502–1503.
[44] H. Fu, L. Zhang, S. Zhang, Y. Zhu, J. Zhao, J. Phys. Chem. B 110 (2006) 3061–3065.
[45] F. Dong, W. Zhao, Z. Wu, S. Guo, J. Hazard. Mater. 162 (2009) 763–770.
[46] F. Dong, Z. Wang, Y. Li, W.K. Ho, S.C. Lee, Environ. Sci. Technol. 48 (2014) 10345–10353.
[47] L. Huang, L. Li, W. Dong, Y. Liu, H. Hou, Environ. Sci. Technol. 42 (2008) 8070–8075.
[48] S. Yamazoe, T. Okumura, Y. Hitomi, T. Shishido, T. Tanaka, J. Phys. Chem. C 111 (2007) 11077–11085.
[49] S. Yamazoe, Y. Hitomi, T. Shishido, T. Tanaka, Appl. Catal. B 82 (2008) 67–76.
[50] S. Yamazoe, T. Okumura, T. Tanaka, Catal. Today 120 (2007) 220–225.
[51] S. Yamazoe, K. Teramura, Y. Hitomi, T. Shishido, T. Tanaka, J. Phys. Chem. C 111 (2007) 14189–14197.
[52] M.A. Kebede, N.K. Scharko, L.E. Appelt, J.D. Raff, J. Phys. Chem. Lett. 4 (2013) 2618–2623.
[53] M.A. Kebede, M.E. Varner, N.K. Scharko, R.B. Gerber, J.D. Raff, J. Am. Chem. Soc. 135 (2013) 8606–8615.